14,08

Effect of electron-beam Ti-Ta surface alloying on the mechanical properties and deformation behavior of the TiNi alloy in cyclic torsion tests

© F.A. D'yachenko, V.V. Loban', V.O. Semin, D.V. Chepelev, M.G. Ostapenko, L.L. Meisner

Institute of Strength Physics and Materials Science, Siberian Branch, Russian Academy of Sciences, Tomsk, Russia

E-mail: dfa@ispms.ru

Received May 14, 2024
Revised May 14, 2024
Accepted June 2, 2024

The dependencies of changes in the mechanical properties and deformation behavior of the TiNi alloy with synthesized Ti-Ni-Ta-based surface alloys with a thickness of $\sim 1-2\,\mu$m were investigated in cyclic torsion tests. The synthesis of surface alloys was carried out by alternating the operations of deposition of a $Ti_{70}Ta_{30}$ and $Ti_{60}Ta_{40}$ (at.%) alloying film and liquid-phase mixing of the film/substrate using a pulsed low-energy high-current electron-beam. It was found that electron-beam synthesis leads to an increase in the stress of martensite shear τ_M by $\sim 10-20$ MPa, in the stress of mechanical hysteresis width $\Delta\tau$ by $\sim 40-75$ MPa, as well as to the ability of the material to accumulate and recover inelastic strain by $\sim 0.2\%$ more compared to initial TiNi alloy. After cyclic torsion tests, subsequent heating of the modified samples to a temperature $T \approx 308 \pm 1$ K leads to the recovery of the accumulated residual strain γ_{total}.

Keywords: Ti-Ni-Ta-based surface alloys, nickel titanium alloy, additive thin-film electron-beam synthesis, torsion tests, superelasticity, mechanical properties, scanning electron microscopy, surface morphology.

DOI: 10.61011/PSS.2024.07.58997.125

1. Introduction

Alloys based on nickel titanium alloy (alloys TiNi), having shape memory effect and superelasticity (SME-SE), are used to manufacture actuators of microelectromechanical systems (MEMS) [1–5], used in operation of miniature products of medical [1–3,5] and nonmedical [4,5] purpose (surgical tools, implants, actuators, temperature sensors, etc.). To improve physical and mechanical properties, radiopacity, corrosion resistance and biocompatibility of TiNi alloys, while maintaining the inelastic characteristics of the alloy (SME-SE) currently ion-beam [6], electron-beam [7], laser [8] and ion-plasma [9–15] methods of surface treatment are used.

The thin-film metal glasses (TFMG) formed on surface of alloys of structural and functional purpose ensure significant increase in corrosion resistance [12] and fatigue characteristics [10,13,14] of substrate materials. The study results [10,13,14] showed that formation of thin ($\leq 1\,\mu$m) amorphous metal coatings on surface of functional (alloys TiNi [10,13]) and structural (stainless steel [13], alloy Ti-6Al-4V [14]) materials facilitates significant increase in fatigue characteristics (fatigue limit, critical stress before failure) of systems [coating/substrate]. However, low mechanical compatibility and strength of the coatings adhesion to the substrate can lead to peeling of the coatings even at small strains ($\leq 1\%$) [15], including during operation on surface of products of alloys TiNi [13].

So, the peeling problems, limited adhesion strength and low mechanical compatibility of TFMG with TiNi-substrate due to presence of interface between them make TFMG unpromising for application to miniature product of alloy TiNi operating at alternating cyclic loading. These problems can be overcome if on surface of TiNi-substrate surface alloys (SAs) [16–20] with given chemical composition (based on systems of Ti, Ni and Ta) and thickness ($\sim 1-2\,\mu$m) are formed using additive thin-film electron-beam synthesis. The essence of this method [16] consists in repeated alternation of operations of deposition of a dopant film of given composition ($Ti_{70-60}Ta_{30-40}$ (at.%) and thickness ($\sim 50-100$ nm)) and liquid-phase mixing of the film components and substrate using a pulsed low-energy (≤ 30 keV) high-current (up to ~ 25 kA) electron-beam (LEHCEB) of microsecond duration ($\sim 2-4\,\mu$s) in single vacuum cycle.

According to study results [16–19], obtained by TEM methods, the synthesized on TiNi-substrate SA based on system Ti-Ni-Ta using the alloying films $Ti_{70}Ta_{30}$ [16–18] and $Ti_{60}Ta_{40}$ [16,19], are characterized by different structure, differ by chemical and phase compositions. The experiments [16–18] showed that using the alloying films $Ti_{70}Ta_{30}$ on surface of alloy TiNi SA is formed with thickness $\sim 1\,\mu$m, which has multilayer nanocomposite (amorphous-nanocrystalline) structure. On the other hand, [16,19] showed that using films $Ti_{60}Ta_{40}$ on surface of alloy TiNi Sa was formed with thickness $\sim 1.8\,\mu$m, which has multilayer amorphous structure. The structural diagrams and detail

description of structural studies of these SAs are given in papers [16–19].

According to the study results obtained by instrumental indentation methods [18,19], the synthesized SA based on system Ti-Ni-Ta have by ~ 2 and ~ 1.5 times higher values of microhardness H and modulus of elasticity E, respectively, than alloy TiNi, but at that with values of elastoplastic parameters close to values of TiNi-substrate. It is shown than due to high plasticity and monotonous measurement of physical and mechanical properties from surface to substrate, SAs have high mechanical compatibility with TiNi-substrate. The studies [16–19] showed that these SAs according to their physical and mechanical (high strength and plasticity [18,19], mechanical compatibility with substrate [18,19]) properties and decreased concentration of nickel [16,17,19] have high potential of use in industry of miniature products of medical and nonmedical purpose as protective barrier layers on surface of alloys TiNi. However, a number of problems arose during the studies [16–19] stay unsolved.

1) Previously studied structural and physical-mechanical properties of SA based on Ti-Ni-Ta were studied on model flat TiNi-samples with simple geometric shape (plane-parallel plates of dimensions $1 \times 10 \times 10$ mm). Behavior of systems [SA/TiNi-substrate] was not studied during mechanical tests of samples-prototypes of miniature products, in particular during cyclic torsion tests.

2) There are no data on SA effect on the mechanical properties and strain behavior of alloy TiNi depending on construction (mono-/multilayer), structure (nanocomposite, amorphous) and physico-mechanical properties of SA.

3) Effect was not determined of SA on the important operation characteristics of alloy, such as: stress of beginning of martensite shear accumulation, stress of mechanical hysteresis, value of reversible inelastic strain, i. e. strain accumulated during loading above the elastic strength and recovered during unloading, value of accumulated residual strain after each cycle of test.

4) SA morphology after mechanical torsion test was not studied. Mechanisms of strain and destruction of systems [SA/TiNi-substrate] were not studied.

So, the present paper objective — during cyclic torsion tests of samples-prototypes of miniature products determine patterns of change in mechanical properties and strain behavior of alloy TiNi with synthesized on its surface SA based on Ti-Ni-Ta (using alloying films $Ti_{70}Ta_{30}$ and $Ti_{60}Ta_{40}$ (at. %)), and also determine the interrelationship of these properties and construction, structure, and physico-mechanical properties of SA.

2. Material, processing and study methods

2.1. Materials and surface preparation methods

Samples were prepared from alloy TiNi grade TH-1, obtained by method of vacuum induction melting on furnace with graphite crucible (MATEK-SPF, Russia). Chemical composition of the alloy: Ti (balance)-55.75 Ni-0.035 O-0.02 C-0.003 N-0.001 H (wt. %). ratio Ti : Ni in phase B2(TiNi) corresponds to composition 49 : 51 (at. %). Temperatures of beginning (M_s, A_s) and completion (M_f, A_f) of direct and reverse martensite transformations B2 $\leftrightarrows$ B19′: $M_s = 288 \pm 2$ K, $M_f = 268 \pm 2$ K, $A_s = 308 \pm 2$ K, $A_f = 313 \pm 2$ K. Samples in form of rectangular parallelepipeds of dimensions $1 \times 1 \times 25$ mm for cyclic torsion tests were cut out by method of electric discharge sawing in water from initial plate semiproduct.

Initial stage of sample surface preparation is chemical etching in solution (composition and concentration of acids in ratio: 3 parts of fluoric acid HNO_3 + 1 part of hydrofluoric acid HF) to remove external oxide layer. Further by method of vibromechanical treatment the samples were finished for ~ 120 hours in vibratory finishing machine SP-A12 (Carlo De Giorgi, Italy). During finishing the filler in form of porcelain cylinders ZSP 3/5 (OTEC, Germany) was used. To wash out the wear products after each ~ 40 hours the samples and filler were washed initially in acetone, and then in running water. Upon the vibromechanical treatment completion ultrasonic cleaning in bath UZV-5.7 TTTs (Sapphire, Russia) with distilled water at $T \approx 298$ K, for $t = 30$ min was performed. Further samples were subjected to electrolitic polishing in solution (3 parts of vinegar acid CH_3COOH +1 part of chloric acid $HClO_4$), for t from ~ 5 to ~ 10 s, at current I from ~ 1 to ~ 3 A and voltage U from ~ 15 to ~ 20 V, with solution cooling in water-ice mixture to $T \approx 278$ K. Then ultrasonic cleaning was performed in bath with distilled water at $T \approx 298$ K, for $t = 30$ min. The samples were dried using lint-free paper and loaded in individual packages. Further samples prepared in such way were marked as TiNi.

2.2. Electron-beam synthesis of surface alloys Ti-Ni-Ta

The surface alloys Ti-Ni-Ta (SA) on samples TiNi were formed in single vacuum cycle on a modified automated set-up „RITM-SP“ (Microsplav, Russia) [21,22]. In set-up work chamber the rectangular samples were secured in attachment such that surface modification was performed simultaneously for two faces. Samples were installed on movable work table, its movement ensured operations of film deposition and its pulse electronic-beam liquid phase mixing with substrate in single vacuum cycle. Then admission was performed, samples were turned over, and two rest faces were treated.

Before SA synthesis to smooth the surface and to homogenize the surface layer the pulse LEHCEB-treatment was applied in the mode of surface melting (energy density of the electron beam was $E_s = 2.5$ J/cm^2, number of treatment pulses was $n = 10$, maximum electron energy $U = 21$ keV, pulse duration $\sim 2-3\,\mu$s). Further, on samples surface by magnetron method, simultaneously from two magnetrons the films $Ti_{70}Ta_{30}$ and $Ti_{60}Ta_{40}$ (at. %)

~ 50 nm thick were deposited by method of sputtering single-component targets of pure elements Ti (99.95 wt.%) and Ta (99.95 wt.%) (Girmet, Russia). Composition of the deposited films was monitored by energy dispersive spectroscopy (silicon drift detector X-ACT (Oxford Instruments, Great Britain)) using LEO EVO 50 (SEM) (Zeiss, Germany) scanning electron microscope at an accelerating voltage of $U = 10$ kV. According to measurements the film composition corresponds to the calculated one ($Ti_{70}Ta_{30}$ and $Ti_{60}Ta_{40}$) with accuracy ± 2 at.%. The films practically did not contain carbon, the oxygen concentration in them did not exceed a few at.%. Liquid phase mixing of the system [Ti-Ta-film/TiNi-substrate] was performed using LEHCEB in mode $E_s = 2$ J/cm^2 and $n = 5$. Number of synthesis cycles „deposition-melting" was repeated 20 times during SA synthesis using film $Ti_{70}Ta_{30}$ and 30 times during SA synthesis using film $Ti_{60}Ta_{40}$. In both cases the temperature of TiNi-substrate did not exceed 473 K by the end of the synthesis. Expected thickness of synthesized SA based on Ti-Ni-Ta (using alloying films $Ti_{70}Ta_{30}$ and $Ti_{60}Ta_{40}$) was ~ 1 and $\sim 1.5\,\mu$m, respectively. Further, SAs synthesized in such way are designated as SA1 and SA2. Samples TiNi after synthesis of SA1 and SA2 on surface of alloy are designated as TiNi-SA1 and TiNi-SA2.

2.3. Cyclic torsion tests

Mechanical torsion test were performed in test machine „NDV-100" (Metrotest, Russia) according to GOST 3565−80 [23]. Set-up control and plotting of strain curves were performed using software „M-Text ACS" (Metrotest, Russia).

Test cycle comprises torsion of sample with permanent speed (70°/ min(4% / min)) up to strain value $\gamma_{\max} = 4\%$. Then, with same speed of rotation in opposite direction the load was removed to zero. Number of test cycles N was 20. Length of sample work part l was ~ 18 mm. Tests were performed at temperature $T \approx 298 \pm 1$ K, clockwise, using strain gauge, for which high limit of measurement of force torque was ~ 10 N*m. Torsion test was applied to 3 samples from groups TiNi, TiNi-SA1 and TiNi-SA2.

Accumulated and recovered strain was registered in form of curves „force torque M — torque angle φ", which were converted in dependences „shear stress τ — torsional strain γ" (Figure 1).

Values of tangential stresses τ were calculated using the following equation

$$\tau = \frac{M \cdot 6}{d^3},$$

where M — force torque, d — arithmetic mean of sample thickness.

Torsional strain γ was determined using the following equation

$$\gamma = \frac{\varphi \cdot d \cdot 0.5}{l \cdot 0.01 \cdot 180^\circ/\pi},$$

where φ — torsion angle, l — sample work length.

By experimental data (curves $\tau - \gamma$, Figure 1) were determined stress of beginning of martensite shear accumulation — τ_M, stress mechanical hysteresis — $\Delta\tau$, value of reversible inelastic strain accumulated under loading over elasticity limit — $\gamma_{1\to2}$ and recovered during unloading — $\gamma_{3\to4}$, value of residual strain accumulated after each test cycle — γ_N, and accumulated after each cycle considering previous cycles — γ_{total}. Then dependences of these parameters on cycle „loading-unloading" N were plotted. After mechanical torsion tests the morphology of SA was studied by SEM method under modes of images obtaining in secondary and back-scattered electrons. The studies were carried out on the equipment of „NANOTECH" Center of Equipment Sharing ISPMS SB RAS (Russia, Tomsk).

3. Results and discussion

3.1. Effect of surface alloys Ti-Ni-Ta on mechanical properties and strain behavior of alloy TiNi during cyclic torsion tests

Papers [16–19] provide sturdy results relating construction, structure and physico-mechanical properties of SA1 and SA2 synthesized on surface of alloy TiNi. Let's consider changes in mechanical properties and strain behavior of alloy during cyclic torsion tests depending on features of structure and properties of SA (SA1 — multilayer nanocomposite composition [16–18], SA2 — monolayer amorphous composition [16,19]).

Figure 2 shows curves of accumulation (under load) and recover (during unloading) of torsional strain ($\gamma_{\max} = 4\%$), obtained at $T \approx 298 \pm 1$ K on samples TiNi (curves *1*), TiNi-SA1 (curves *2*) and TiNi-SA2 (curves *3*) depending

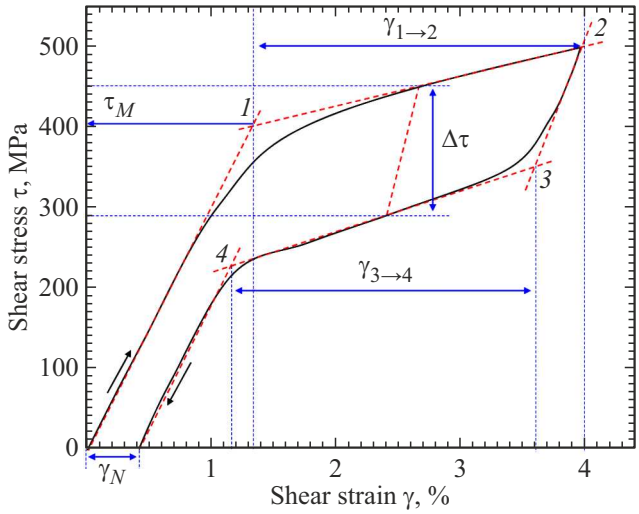

Figure 1. View of curves „shear stress τ — torsional strain γ", where τ_M — stress of beginning of martensite shear accumulation, $\Delta\tau$ — mechanical hysteresis of stress; $\gamma_{1\to2}$ and $\gamma_{3\to4}$ — value of reversible inelastic strain accumulated under loading over elasticity limit and recovered during unloading, γ_N — value of residual strain after each cycle of „loading-unloading" N.

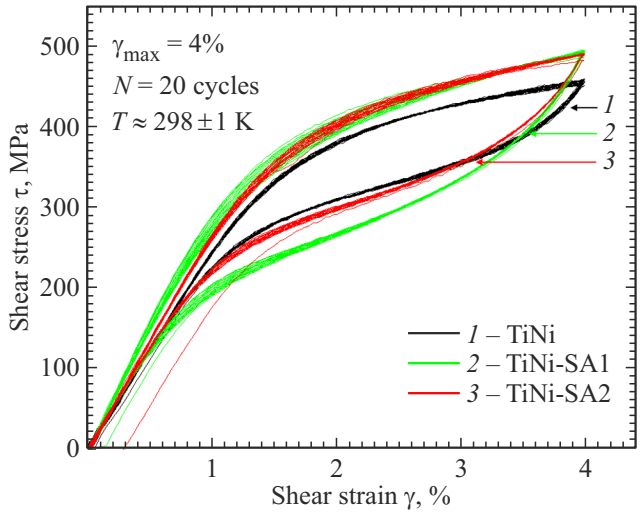

Figure 2. Curves „shear stress τ — torsional strain γ", obtained during cyclic torsion tests for samples: *1* — TiNi; *2* — TiNi-SA1; *3* — TiNi-SA2.

on cycle „loading-unloading" N from 1 to 20. By these diagrams we determined parameters characterizing mechanical properties — stress of beginning of martensite shear accumulation — τ_M (Figure 3, *a*), stress mechanical hysteresis — $\Delta\tau$ (Figure 3, *b*), value of reversible inelastic strain accumulated under loading over elasticity limit — $\gamma_{1\to2}$ (Figure 4, *a*) and recovered during unloading — $\gamma_{3\to4}$ (Figure 4, *b*), value of residual strain accumulated after each test cycle — γ_N (Figure 5, a), and accumulated after each cycle considering previous cycles — γ_{total} (Figure 5, *b*). Figures 3–5 separately shows confidence ranges of values change of studied parameters.

Figure 2 shows that in samples TiNi (curves *1*) loops of strain accumulation and recover have „flag-like" shape with narrow hysteresis typical for alloys TiNi with SE effect [1,2]. Loops shape is repeated during accumulation N from 1 to 20. In samples TiNi-SA1 (curves *2*) and TiNi-SA2 (curves *3*) curves $\tau - \gamma$ have shape close to „flag-like" shape in curves of samples TiNi. Shape of loops changes during accumulation N from 1 to 10, then repeat at N from ~ 10 to 20. It is obvious that despite low ($\sim 1-2\,\mu$m) thickness of SA and their effect on physico-mechanical properties of alloy TiNi to depth $\geq 1\,\mu$m [18,19], the synthesized SA affected the strain behavior and mechanical properties of the alloy TiNi. Firstly, after SA synthesis inclination of curves changed during stages of accumulation and recover of reversible inelastic strain. Secondly, during first ~ 10 cycles the stresses of beginning of martensite shear accumulation τ_M in SA samples were higher by $\sim 10-20$ MPa (Figure 3, *a*, curves *2* and *3*), and higher by $\sim 5-15$ MPa on average (for all cycles) than in samples TiNi (Figure 3, *a*, curve *1*). Thirdly, in samples with SA width of stresses mechanical hysteresis $\Delta\tau$ increased by $\sim 40-75$ MPa (Figure 3, *b*, curves *2* and *3*), relative to samples TiNi (Figure 3, *b*, curve *1*). But in case of samples TiNi-SA2 shape of loops of strain accumulation and recover changes weakly, while in case of samples TiNi-SA1 changes in curves $\tau - \gamma$ and in mechanical properties were significant. Let's consider changes and difference in mechanical properties in samples TiNi, TiNi-SA1 and TiNi-SA2, that differ by construction, structure and physico-mechanical properties.

In samples TiNi upon N accumulation from 1 to ~ 10 stresses are $\tau_M \approx 394$ MPa (Figure 3, *a*, curve *1*). After ~ 10 test cycles dependence $\tau_M(N)$ reaches plateau, and parameter $\tau_M \approx 391$ MPa. It was previously showed that in samples with SA stresses τ_M were higher than in samples TiNi. In both cases with N increasing to 20 we observed linear decreasing of values τ_M to ~ 380 and ~ 398 MPa in samples TiNi-SA1 and TiNi-SA2, respectively (Figure 3, *a*, curves *2* and *3*). Upon N accumulation from 1 to ~ 10 in samples with SA the inclination of curves $\tau_M(N)$ is higher than in samples TiNi. But, upon N accumulation from 10 to ~ 20 in samples TiNi-SA1 values τ_M decrease

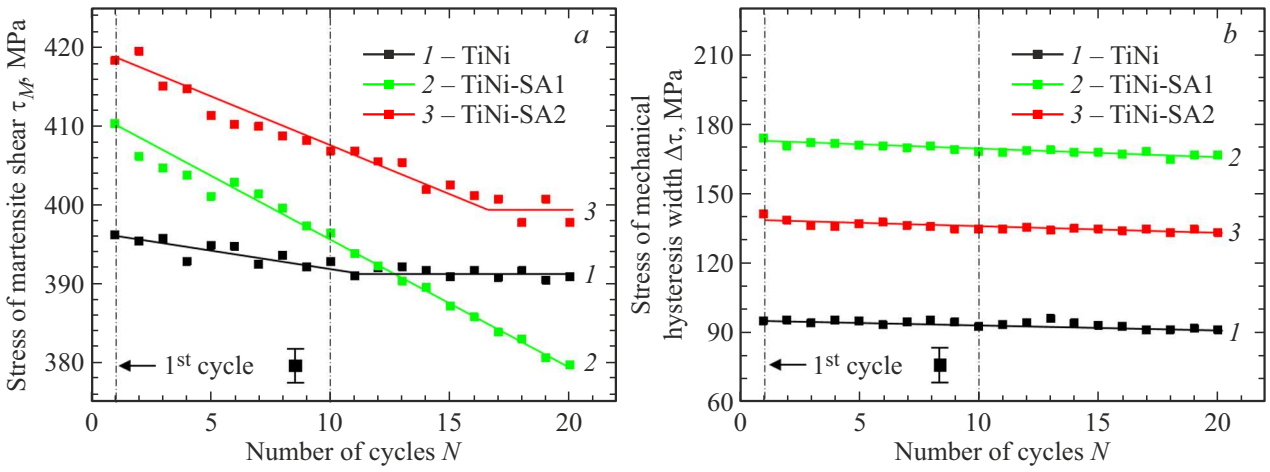

Figure 3. Dependence of stress of beginning of martensite shear accumulation τ_M (*a*) and stress mechanical hysteresis $\Delta\tau$ (*b*) on number of cycles „loading-unloading" N for samples: *1* — TiNi; *2* — TiNi-SA1; *3* — TiNi-SA2.

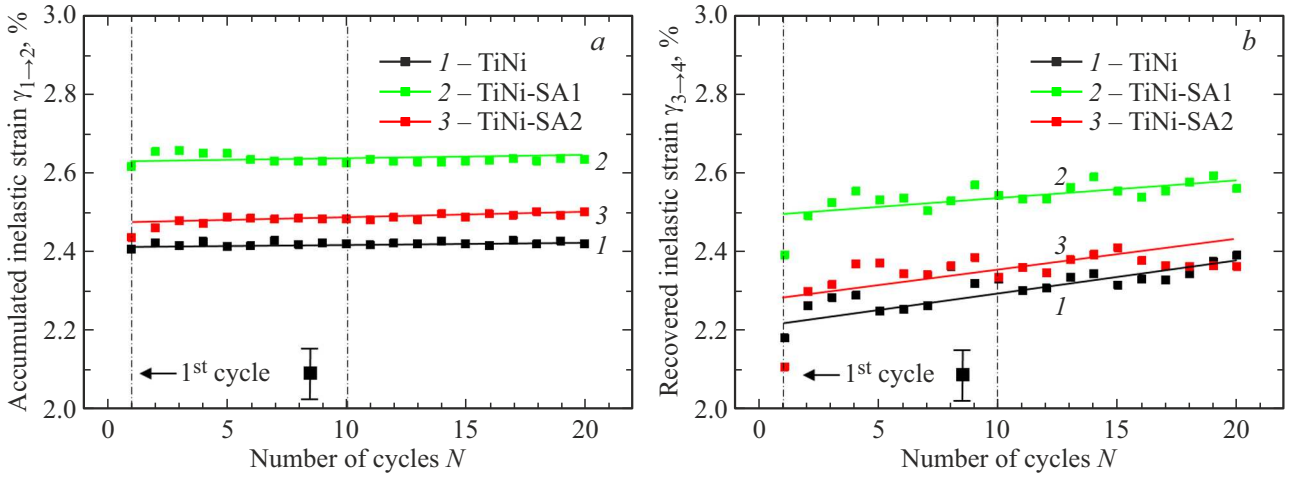

Figure 4. Dependence of reversible inelastic strain accumulated during loading $\gamma_{1\to2}$ (*a*) and recovered during unloading $\gamma_{3\to4}$ (*b*) on number of cycles „loading-unloading" N for samples: *1* — TiNi; *2* — TiNi-SA1; *3* — TiNi-SA2.

by $\sim 5-10$ MPa, as compared to samples TiNi. In samples TiNi-SA2 same decrease in values τ_M finishes after ~ 15 cycles, and value τ_M stays higher by ~ 10 MPa than in samples TiNi. Analysis of the parameter $\Delta\tau$ in curves $\tau-\gamma$ showed (Figure 3, *b*, curves *1–3*), that in samples TiNi, TiNi-SA1 and TiNi-SA2 average (over all cycles) values $\Delta\tau$ are ~ 94, ~ 169 and ~ 135 MPa, respectively. For all samples during N accumulation from 1 to 20 the dependences $\Delta\tau(N)$ are linear.

Considering that under same test conditions the samples TiNi, TiNi-SA1 and TiNi-SA2 differ by structure and properties of surface layers of micron thickness, the identified differences in values of parameters τ_M and $\Delta\tau$ and patters of their change, presumably, are due to difference in their surface structure and properties. τ_M increasing in samples TiNi-SA2, as compared to samples TiNi-SA1, can be due to that SA2 has completely amorphous surface layer $\sim 1.8\,\mu$m thick [16,19], which on surface (≤ 500 nm) is characterized by high values of parameters of microhardness $H \approx 7$ GPa and modulus of elasticity $E \approx 86.5$ GPa [19], as compared to SA1. This means that at stage of elastic accumulation of torsional strain more higher torque shall be applied to samples TiNi-SA2 than in case of samples TiNi. And by contrast, in samples TiNi-SA1, where SA1 is characterized by lower thickness ($\sim 1\,\mu$m) and by multilayer nanocomposite structure [17], with high parameters $H \approx 7.5$ GPa and $E \approx 90$ GPa [18], τ_M increasing is observed only during N accumulation from 1 to ~ 10. Further τ_M decreasing is probably associated with that in samples TiNi-SA1 between SA and TiNi-substrate there is intermediate diffusion zone ($\sim 1\,\mu$m thick) [17], where below located nanocrystalline sublayers have high elasticity $\delta \approx 70\%$ [18] (in paper [18] values of plasticity parameter δ are calculated as per data of instrumented indentation using Yu.V. Milman method [24]).

Figure 4 shows dependences of value of reversible inelastic strain accumulated during loading $\gamma_{1\to2}$ (Figure 4, *a*) and recovered during unloading $\gamma_{3\to4}$ (Figure 4, *b*), on number of cycles N in samples TiNi (curves *1*), TiNi-SA1 (curves 2) and TiNi-SA2 (curves *3*), respectively. In samples TiNi values of accumulated $\gamma_{1\to2}$ and recovered $\gamma_{3\to4}$ strain differ by $\sim 0.1\%$ during number of cycles N accumulation from 1 to ~ 10 (curves *1*), and practically coincide upon reaching 20-th cycle, i.e. $\gamma_{1\to2} \approx \gamma_{3\to4}$. In samples TiNi-SA1 (curves *2*) values $\gamma_{1\to2}$ and $\gamma_{3\to4}$ are higher than in samples TiNi. During first ~ 10 test cycles there is divergence between branches of accumulation and recover in $\sim 0.15\%$. When reaching 20-th cycle this divergence decreases to $\sim 0.05\%$. In samples TiNi-SA2 (curves *3*) values $\gamma_{1\to2}$ and $\gamma_{3\to4}$ are lower than in samples TiNi-SA1, but higher than in samples TiNi. So, during first ~ 10 test cycles there is divergence between $\gamma_{1\to2}$ and $\gamma_{3\to4}$ by $\sim 0.2\%$. After 20 cycles this divergence keeps at level of $\sim 0.1\%$. Identified divergence between $\gamma_{1\to2}$ and $\gamma_{3\to4}$ in samples TiNi-SA2 is linked with that this SA having high strength amorphous structure and lower plasticity $\delta \approx 60\%$ [19], probably, starts cracking during first loading cycles. In other words, as a result of cracking, SA2 began to have a lesser effect on the integral inelastic properties of the TiNi substrate.

In both cases the analysis of reversible inelastic strain accumulated during loading $\gamma_{1\to2}$ and recovered during unloading $\gamma_{3\to4}$ shows that SA presence results in increase in inelastic properties of the substrate materials. This is confirmed by average (over all cycles) values $\gamma_{1\to2}$ and $\gamma_{3\to4}$, calculated during loading and unloading: ~ 2.4 and 2.3% (in samples TiNi), ~ 2.6 and 2.5% (in samples TiNi-SA1), ~ 2.5 and 2.3% (in samples TiNi-SA2). In other words, the surface modification resulted in increase in the duration of the stage of accumulation and recover of inelastic strain on the curves $\tau-\gamma$. However, samples with SA during first ~ 10 cycles demonstrate higher by $\sim 0.05-0.1\%$ divergence of branches of accumulation and recover of strain than in samples TiNi. When 20-th cycles is reached this divergence practically absent entirely in

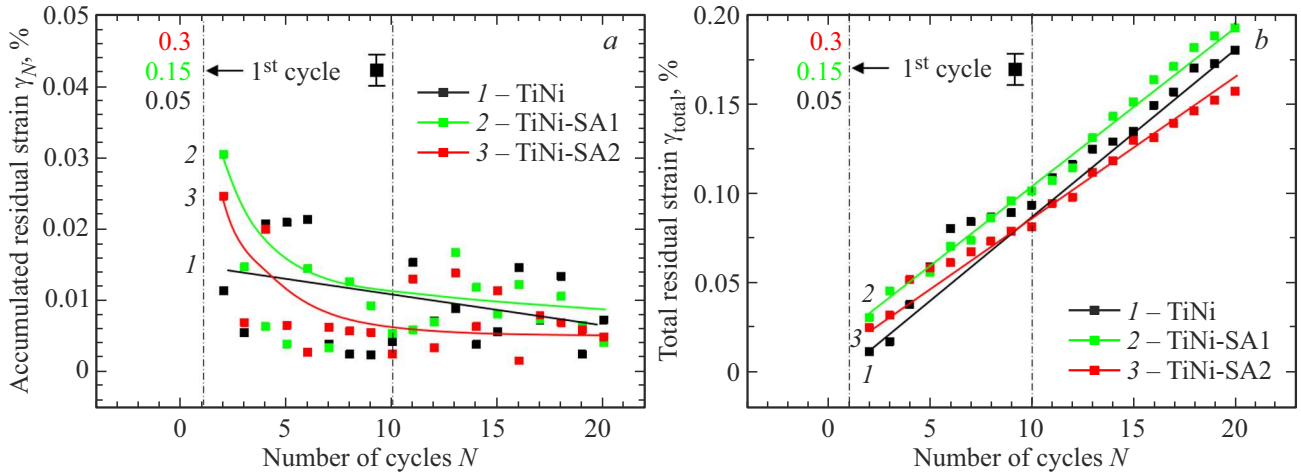

Figure 5. Dependence of residual strain accumulated after each test cycle γ_N (a) and accumulated after each cycle considering previous cycles γ_{total} (b) on number of cycles N for samples: *1* — TiNi; *2* — TiNi-SA1; *3* — TiNi-SA2.

samples TiNi-SA1, and in samples TiNi-SA2 it present and is $\sim 0.1\%$.

The obtained results show that despite presence in SA by ~ 2 and ~ 1.5 times higher values of microhardness and modulus of elasticity [18,19] as compared to TiNi-substrate, and their effect on mechanical properties of alloy TiNi (τ_M higher by $\sim 10-20$ MPa (Figure 3, a), $\Delta\tau$ higher by $\sim 40-75$ MPa (Figure 3, b)), the electron-beam synthesis of SA resulted in increased inelastic properties of alloy TiNi, i.e. increase in accumulation and recover of inelastic strain by $\sim 0.2\%$. This effect can be explained by the fact that, as it was explained earlier, at stage of elastic accumulation of torsional strain more higher torque shall be applied to strengthened samples with SA than in case of samples TiNi. In turn, this resulted in fact that in the process of accumulation and recover of reversible inelastic strain in samples with SA, a large volume fraction of TiNi-substrate material was involved, where reversible martensite B2 $\rightleftarrows$ B19′ transformation occurred, this resulted in increase in portions of accumulated $\gamma_{1\to2}$ and recovered $\gamma_{3\to4}$ components of torsional strain.

Figure 5 shows dependences of residual strain accumulated after each test cycle γ_N (Figure 5, a), and accumulated after each cycle considering previous cycles γ_{total} (Figure 5, b) in samples TiNi (curves *1*), TiNi-SA1 (curves *2*) and TiNi-SA2 (curves *3*). Figure 5, a, b, separately, show values of γ_N at $N = 1$, which are ~ 0.05, ~ 0.15 and $\sim 0.3\%$ in samples TiNi, TiNi-SA1 and TiNi-SA2, respectively. In samples TiNi-SA1 and TiNi-SA2 γ_N increasing at $N = 1$ can say about SA cracking resulted in incomplete recover of residual strain. In all samples strain γ_N on average (over all cycles, not considering data for $N = 1$) is $\sim 0.01\%$. The obtained result shows that in samples with SA, excluding first test cycle, accumulation of the residual strain after each cycles is close to values γ_N in samples TiNi. Figure 5, b shows that after 20 cycles accumulation in samples TiNi-SA1 and TiNi-SA2 the level of the accumulated strain γ_{total} is ~ 0.19 and $\sim 0.16\%$ (not considering data for $N = 1$), respectively. In samples TiNi after 20 cycles $\gamma_{total} \approx 0.18\%$ (not considering data for $N = 1$). The obtained result shows that electron-beam synthesis of SA does not result in increase in accumulation of the residual strain during cyclic torsion tests.

It is important to note that incomplete recover of strain during N accumulation from 1 to 20, observed in samples TiNi, TiNi-SA1 and TiNi-SA2 (considering data for $N = 1$), which is ~ 0.23, ~ 0.34 and $\sim 0.44\%$, respectively, is probably determined by the presence of residual portion of martensite phase,which presence in alloy TiNi of this composition is possible at $T \approx 298 \pm 1$ K. Upon cyclic tests completion the next heating of all samples to temperature $T \approx 308 \pm 1$ K results in recover of the residual strain, which is allowed for biomedical application of the alloy TiNi [1–5].

3.2. Electron microscopy studies of surface morphology of surface alloys Ti-Ni-Ta after cyclic torsion test

Upon mechanical test completion the important step of the performed studies is study of mechanisms of strain and destruction of synthesized SA1 and SA2 depending on features of the construction, structure and physico-mechanical properties. One of stages of such studies is identification of discontinuities of surface layers, analysis of chips and cracks on surface, search of regions with SA peeling from substrate material.

Figure 6 shows SEM-images of surface of samples TiNi before (Figure 6, a) and after (Figure 6, b, c) cyclic torsion test ($\gamma_{max} = 4\%$, $N = 20$, $T = 298 \pm 1$ K). Figure 6, a shows that before SA synthesis the surface of samples TiNi, prepared for use of methods of vibromechanical and electrochemical treatments, is homogeneous, without notches and slag on faces, which occurred after electric

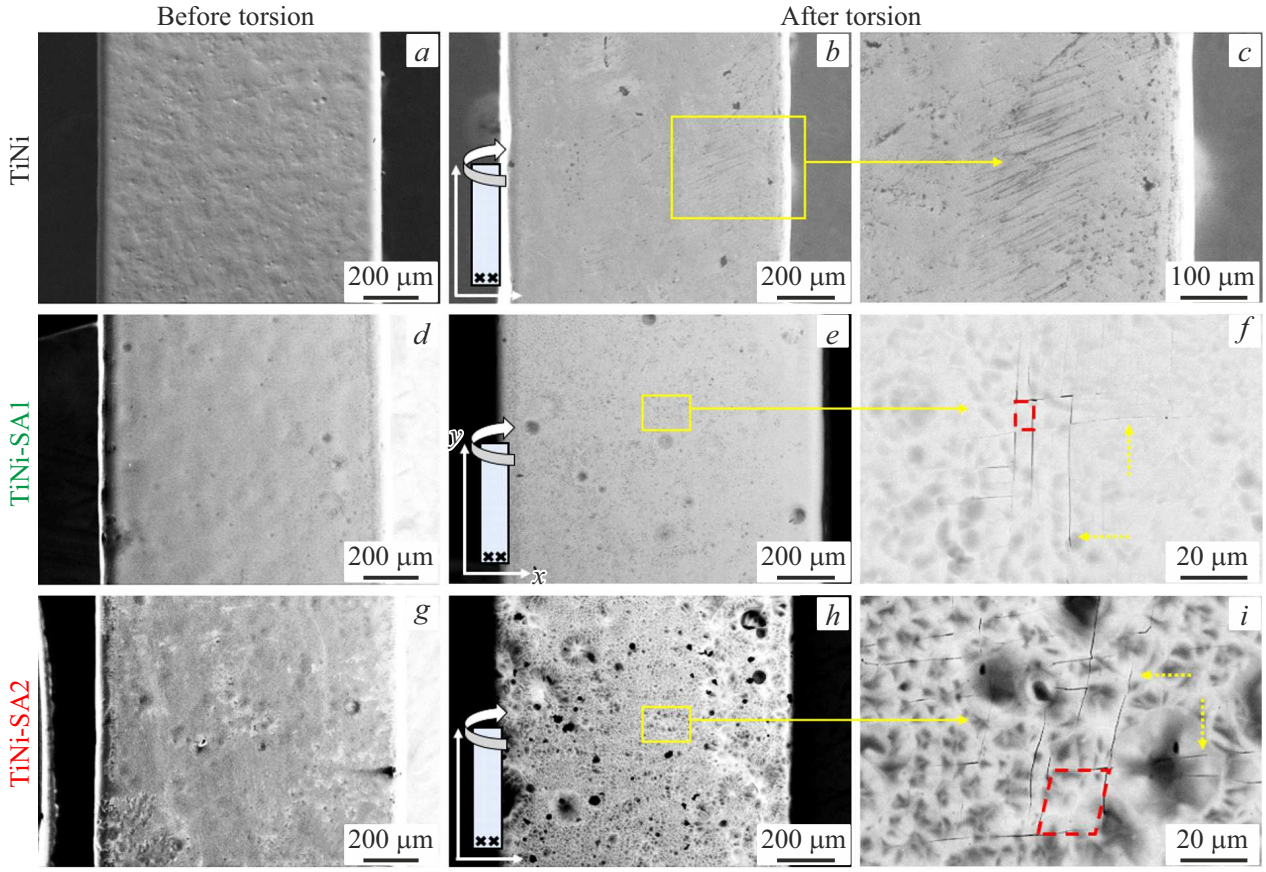

Figure 6. SEM-images of sample surface before (a, d, g) and after (b, c, e, f, h, i) cyclic torsion test ($\gamma_{max} = 4\%$, $N = 20$, $T = 298 \pm 1$ K): a–c — TiNi; d–f — TiNi-SA1; g–i — TiNi-SA2.

discharge sawing. Preliminary treatments of surface resulted in smoothing of edges of rectangular samples. After cyclic test we determined (Figure 6, *b, c*) that on surfaces of samples TiNi there were regions containing sliding bands at angle to the torsion axis of the sample. Average length of bands is $\sim 100\,\mu$m. No chips and cracks are observed on surface of samples TiNi.

Figure 6 shows SEM-images of surface of samples TiNi-SA1 (Figure 6, *d*–*f*) and TiNi-SA2 (Figure 6, *g*–*i*) before and after cyclic torsion test. Analysis of morphology and topography of surfaces of SA1 and SA2, previously made on samples in form of plane-parallel plates ($1 \times 10 \times 10$ mm), showed [16] that the electron-beam method ensures synthesis of both SAs with homogeneous and smoothed morphology of surface. During such SAs synthesis on rectangular samples ($1 \times 1 \times 25$ mm) similar result is achieved (Figure 6, *d, g*). Note that SA morphology is homogeneous not only on faces but in region of edges of samples. After SA electron-beam synthesis no cracks are determined on surface of samples TiNi-SA1 and TiNi-SA2.

When studying samples TiNi-SA1 after cyclic torsion test we determined that on all faces the surface of samples is homogeneous (Figure 6, *e*), without microscopic discontinuities of SA integrity. Detailed SEM analysis of the surface at high magnifications showed that local regions with microcracks formed on the surface (Figure 6, *f*). Microcracks are oriented along mutually orthogonal directions — in the longitudinal and transverse directions relative to the torsion axis of the sample (*indicated by dashed arrows*). Microcracks form cellular grid, where the shape of the grid elements (cells) — *rectangular (highlighted by the dashed line)*. Microcracks are located only on faces of work portion of rectangular samples and do not extend to edges. No signs of SA1 peeling from TiNi-substrate are determined.

After tests of samples TiNi-SA2 it was determined that on all faces the samples surface is homogeneous (Figure 6, *h*). At that on surface similar local regions with microcracks were formed (Figure 6, *i*). Microcracks are oriented in longitudinal and transverse directions relative to the torsion axis of the sample (*indicated by dashed arrows*). However, in the longitudinal direction the microcracks are located at angle to the torsion axis. The microcracks form a cellular grid and do not extend to the edges of the samples. No signs of SA2 peeling from TiNi-substrate are determined.

So, after cyclic torsion tests there are differences between destruction of samples TiNi with SA1 and SA2: 1) in samples TiNi-SA2 cracks in longitudinal direction are located at large angle to the torsion axis of sample; 2) in samples TiNi-SA2 regions with microcracks have large dimensions,

and shape of grid elements changed from rectangular to *parallelograms* (Figure 6, *i*, *shown by dashed line*).

As per data the formation of large regions of TiNi-SA2 cracking is associated, by our opinion, with the following reasons [16,19]: 1) amorphous structure of SA2; 2) large thickness ($\sim 1.8\,\mu$m); 3) surface (≤ 500 nm) layer is characterized by high values of modulus of elasticity $E \approx 86.5$ GPa and low plasticity $\delta \approx 60\%$, and 4) by high values of stress martensite shear accumulation τ_M during first cycles ($\tau_M \approx 418$ MPa, Figure 3, *a*, curve *3*). This means that application of larger force torque to ordered samples TiNi-SA2 resulted in cracking of amorphous SA2 at stage of elastic accumulation of torsional strain during first loading cycles. Due to the obtained results there are grounds to suppose effect of scale factor on properties of the system [amorphous SA/TiNi-substrate]. In other words, the possibility of reducing the thickness of amorphous SA2 seems promising, which will: 1) facilitate in its fracture resistance increasing; 2) ensure properties improvement of miniature products (≤ 1 mm) of alloy TiNi without critical effect on the integral inelastic properties (SME-SE) of TiNi-substrate.

On the other hand, in samples TiNi-SA1, with lesser thickness of SA1 ($\sim 1\,\mu$m), multilayer construction of it is nano composite despite high parameters $H \approx 7.5$ GPa and $E \approx 90$ GPa in surface (≤ 500 nm) layer, lesser surface cracking is associated with presence of intermediate diffusion zone (thickness $\sim 1\,\mu$m), where the laying below nanocrystalline sublayers have high plasticity ($\delta \approx 70\%$) [16–18]. In turn, determined differences in nature of destruction of SA1 and SA2, namely in change of grid elements (cells) in regions with microcracks (Figure 6, *f, i*), can be associated with difference in structure and properties of SA1 and SA2.

Thus, electron microscopy studies showed that surface alloys Ti-Ni-Ta synthesized on surface of samples TiNi in form of parallelepipeds doe not peel from TiNi-substrate after cyclic torsion test ($\gamma_{\max} = 4\%$, $N = 20$, $T = 298 \pm 1$ K). Depending on construction, structure and properties of SA on samples surface the local regions with microcracks were formed, they were oriented at different angles along directions relative to torsion axis of sample. Microcracks are located only on faces of work portion of rectangular samples and do not extend to edges.

4. Conclusion

In this paper, surface alloys based on the Ti-Ni-Ta system were synthesized using the additive thin-film electron-beam method on the surface of TiNi samples in the form of rectangular parallelepipeds using alloying films $Ti_{70}Ta_{30}$ and $Ti_{60}Ta_{40}$ (at.%). The effect of construction, structure and properties of surface alloys Ti-Ni-Ta on mechanical properties and strain behavior of alloy TiNi during cyclic torsion tests were studied. It is shows that surface alloys Ti-Ni-Ta have no critical effect on integral properties of TiNi-substrate, but by contrast result in increase of inelastic characteristics of samples-prototypes of the miniature products of alloy TiNi. Based on data obtained during torsion tests and by method of scanning electron microscopy the conclusions are made.

1. Evaluation of stress of martensite shear accumulation τ_M and stresses of mechanical hysteresis width $\Delta\tau$ shows that electron-beam synthesis results in increase of parameters τ_M by $\sim 10-20$ MPa and $\Delta\tau$ by $\sim 40-75$ MPa as compared to samples TiNi without irradiation and alloying.

2. Evaluation of dependences of values of reversible inelastic strain accumulated during loading above elastic limit $\gamma_{1\to2}$ and recovered during unloading $\gamma_{3\to4}$ shows that the electron-beam synthesis results in $\sim 0.2\%$ increase in ability of the material to accumulate and recover inelastic strain.

3. Synthesis of surface alloys Ti-Ni-Ta does not result in increase in residual strain γ_N, accumulated after each cycler „loading-unloading" N. In modified samples the strain γ_N on average (over all cycles, not considering data for $N = 1$) is $\sim 0.01\%$, this corresponds to values for samples TiNi without irradiation and alloying. Upon completion of cyclic torsion test the next heating of modified samples to temperature $T \approx 308 \pm 1$ K results in recovery of residual strain γ_{total}.

4. Electron microscopy studies show that after cyclic torsion test the surface alloys Ti-Ni-Ta do not peel from TiNi-substrate. On surface of modified samples the local regions were formed with microcracks which depending on type of structure of surface alloy and its properties have different dimensions and orientation of cracks relative to torsion axis of sample.

The results obtained are of practical significance, since they allow us to establish that for miniature (≤ 1 mm) products of medical and nonmedical purpose manufactured from alloys TiNi to improve physico-mechanical properties, radiopacity, corrosion resistance and biocompatibility of these alloys, an electron beam method for the synthesis of surface Ti-Ni-Ta alloys is suitable, which complies with the requirements of high reversibility of strain of alloys TiNi in narrow mechanical or temperature range.

Funding

This study was carried out by the Government research assignment for Institute of Strength Physics and Materials Science, project FWRW-2021-0003.

Conflict of interest

The authors declare that they have no conflict of interest.

References

[1] N. Sabahi, W. Chen, C.-H. Wang, J.J. Kruzic, X. Li. JOM **72**, 1229 (2020). DOI: 10.1007/s11837-020-04013-x
[2] J. Zhu, Q. Zeng, T. Fu. Corros. Rev. **37**, 539 (2019). DOI: 10.1515/corrrev-2018-0104
[3] U. Roshan, R. Amarasinghe, N. Dayananda. J. Rob. Networking Artif. Life **5**, 194 (2018). DOI: 10.2991/jrnal.2018.5.3.11

[4] M. Mehrpouya, H.C. Bidsorkhi. Micro Nanosyst. **8**, 79 (2016). DOI: 10.2174/1876402908666161102151453
[5] J.J. Mohd, M. Leary, A. Subic, M.A. Gibson. Mater. Des. **56**, 1078 (2014). DOI: 10.1016/j.matdes.2013.11.084
[6] C. Yan, Q. Zeng, W. He, J. Zhu. Tribol. Int. **155**, 106816 (2021). DOI: 10.1016/j.triboint.2020.106816
[7] S.N. Meisner, I.V. Vlasov, E.V. Yakovlev, S.V. Panin, L.L. Meisner, F.A. D'yachenko. Mater. Sci. Eng. A **740-741**, 381 (2019). DOI: 10.1016/j.msea.2018.10.113
[8] A. Pequegnat, A. Michael, J. Wang, K. Lian, Y. Zhou, M.I. Khan. Mater. Sci. Eng. C **50**, 367 (2015). DOI: 10.1016/j.msec.2015.01.085
[9] E.S. Marchenko, Yu.F. Yasenchuk, S.V. Gunther, G.A. Baigonakova, O.V. Kokorev, A.A. Shishelova, O.A. Fatyushina. Russ. Phys. J. **62**, 1789 (2020). DOI: 10.1007/s11182-020-01907-w
[10] C.-W. Chi, Y.-L. Deng, J.-W. Lee, C.-P. Lin. J. Formosan Med. Associat. **116**, 373 (2017). DOI: 10.1016/j.jfma.2016.07.003
[11] C. Park, S. Kim, H.-E. Kim, T.-S. Jang. Surf. Coat. Technol. **305**, 139 (2016). DOI: 10.1016/j.surfcoat.2016.08.014
[12] P. Yiu, W. Diyatmika, N. Bonninghoff, Y.-C. Lu, B.-Z. Lai, J.P. Chu. J. Appl. Phys. **127**, 030901 (2020). DOI: 10.1063/1.5122884
[13] H. Jia, F. Liu, Z. An, W. Li, G. Wang, J.P. Chu, J.S.C. Jang, Y. Gao, P.K. Liaw. Thin Solid Films **561**, 2 (2014). DOI: 10.1016/j.tsf.2013.12.024
[14] C.M. Lee, J.P. Chu, W.Z. Chang, J.W. Lee, J.S.C. Jang, P.K. Liaw. Thin Solid Films **561**, 33 (2014). DOI: 10.1016/j.tsf.2013.08.027
[15] S. Shabalovskaya, J. Anderegg, J. van Humbeeck. Acta Biomater. **4**, 447 (2008). DOI: 10.1016/j.actbio.2008.01.013
[16] Patent № 2017137653/15(065731) RF, MPK A61L 27/06, B82B 1/00, C22C 45/10, A61L 31/18, C22C 45/04, C23C 28/00. Sposob sinteza rengenokontrastnogo poverkhnostnogo Ti-Ta-Ni splava s amorphnoj ili amorfo-nanokristallicheskoj strukturoj na podlozhke iz TiNi splava. L.L. Meisner, A.B. Markov, G.E. Ozur, V.P. Rotshtein, S.N. Meisner, E.V. Yakovlev, E.Yu. Gudimova, V.O. Semin, Patentoobladatel' IFPM SO RAN, ISE SO RAN. Opubl. 11.04.18. (in Russian)
[17] L.L. Meisner, A.B. Markov, V.P. Rotshtein, G.E. Ozur, S.N. Meisner, E.V. Yakovlev, V.O. Semin, Yu.P. Mironov, T.M. Poletika, S.L. Girsova, D.A. Shepel. J. Alloys Compd. **730**, 376 (2018). DOI: 10.1016/j.jallcom.2017.09.238
[18] S.N. Meisner, E.V. Yakovlev, V.O. Semin, L.L. Meisner, V.P. Rotshtein, A.A. Neiman, F. D'yachenko. Appl. Surf. Sci. **437**, 217 (2018). DOI: 10.1016/j.apsusc.2017.12.107
[19] F.A. D'yachenko, V.O. Semin, M.G. Ostapenko, L.L. Meisner. Phys. Solid State **65**, 593 (2023). DOI: 10.21883/PSS.2023.04.56000.24.
[20] M.G. Ostapenko, V.O. Semin, L.L. Meisner, F.A. D'yachenko, S.N. Meisner, E.M. Oks, K.P. Savkin, A.B. Markov, E.V. Yakovlev, S.I. Yuzhakova, D.V. Chepelev, V.V. Loban'. Russ. Phys. J. **66**, 503 (2023). DOI: 10.1007/s11182-023-02968-3
[21] G.E. Ozur, D.I. Proskurovsky. Plasma Phys. Rep., **44**, 18 (2018). DOI: 10.1134/S1063780X18010130.
[22] A.B. Markov, A.V. Mikov, G.E. Ozur, A.G. Padei. Instrum. Exp. Tech., **54**, 862 (2011). DOI: 10.1134/S0020441211050149.
[23] GOST 3565−80 Metally. Metod ispytanij na kruchenie. Izd-vo standartov/ (1980). 17 p. (in Russian).
[24] Yu.V. Milman. J. Phys. D **41**, 074013 (2008). DOI: 10.1088/0022-3727/41/7/074013

Translated by I.Mazurov